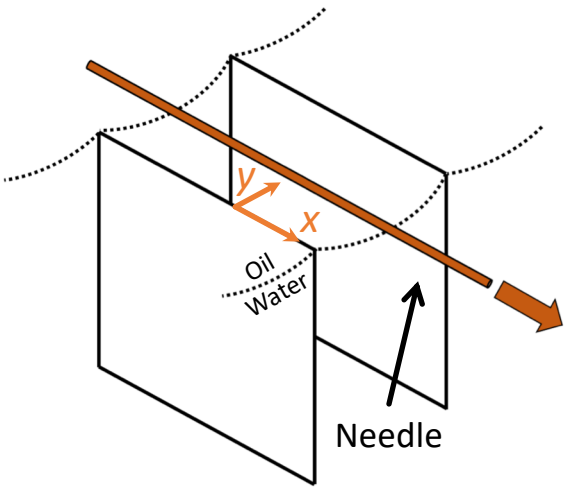

Figure 1: **Interfacial Stress Rheometer** Sketch of interfacial stress rheometer (ISR). Dense colloidal monolayer sits on water-oil interface that is bounded by two upright parallel glass walls. A thin magnetic needle cyclically shears the monolayer using Helmholtz coils. Accurate rheometry is obtained by tracking needle position as a function of forcing; particle tracking is used to characterize material microstructure.

6 Supplemental materials

6.1 Discussion of systems

Here we make a few comments on the breadth of properties covered by our systems (as summarized in table 4). First, we note that the systems studied span a large range of disorder, ranging from crystalline regions of several hundred particles (Fig. 2a) to merely a few (Fig. 2d). Second we note that, Lennard-Jones potentials are attractive at long distances. So our results hold for systems where some of the particles experience attraction, as long as the system is jammed. Finally, our systems span a wide range of length scales. Lennard-Jones systems are atomic scale.

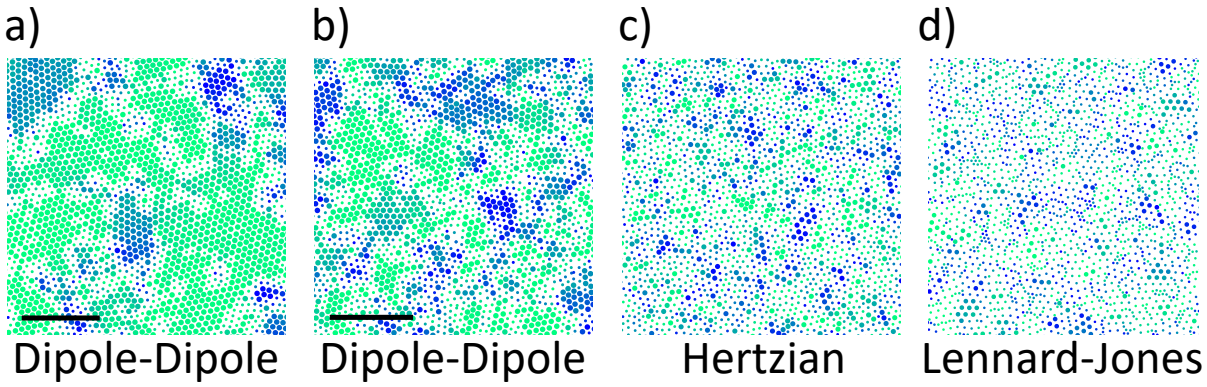

Figure 2: **Disorder increasing left to right** Crystalline regions visualized via sixfold bond orientation order, Ψ_6, measured from particle positions. Size of crystals decreases from left to right, indicating an increase in disorder. Colors help to indicate the lattice director (orientation) as a guide for the eye to help discern ordered and disordered domains. Dots with large size indicate $|\Psi_6| > 0.9$, and small dot size indicates $|\Psi_6| < 0.9$. (Scale bars: $100\mu m$). a) Mono-disperse, dipole-dipole, experimental system B. b) Bi-disperse, dipole-dipole, experimental system A. c) Bi-disperse, Hertzian, simulation system D. d) Bi-disperse, Lennard-Jones, simulation system C.

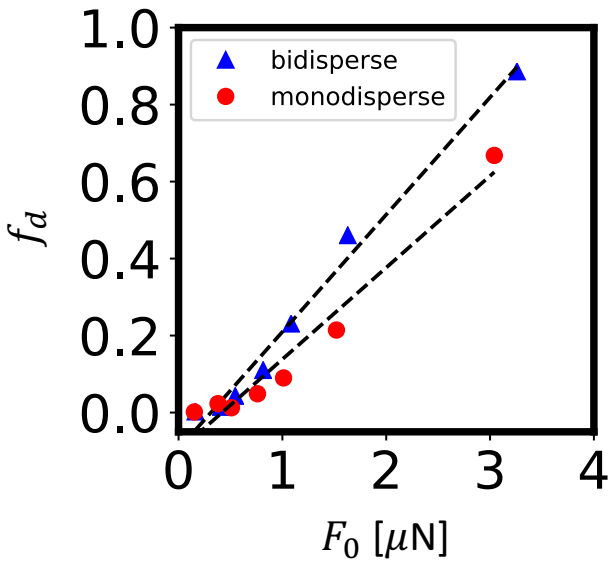

Figure 3: **Imposed force scales with fraction of dissipative events.** Within the linear rheology regime studied, the fraction of particles undergoing non-affine, disspative events scales linearly with the imposed force on the system. The dashed lines (- - -) are added to guide the eye.

Dipole-dipole systems are colloidal scale. Hertzian systems are granular scale. One further difference among our systems is that our experiments include an intermediary fluid and an interface, whereas our simulations do not. This serves to explore the role of specific energy dissipation (viscous drag in the experiments) versus unspecific dissipation (the simulations).

6.2 Scaling of imposed force and non-affine events

In the main text we identify that the entropic ratio $s_{2,h}$ varies as a quadratic in figure 4a. Our model, (main body equation 2), makes no prediction about the form of the scaling unless we know how force amplitude, F_0, and the fraction of particles undergoing dissipative events, f_d, scale with each other. These values scale linearly with each other in our experiments (Fig. 3), which results in a quadratic scaling. This is an approximation, as at very high strain amplitudes it is expected that the fraction of non-affine events will plateau at unity. But within the linear rheological regime studied here, this limit is not reached.

6.3 Experimental potentials

In this section we describe our method of estimating the mean inter-particle potential of our experimental systems A and B. Sulfate latex spheres of $D_l = 5.6\mu m$ and $D_s = 4.1\mu m$ are adsorbed at an interface of decane and water. The sulfate latex groups cover the surfaces of the particles, providing a charge. The charges and the presence of the interface cause the particles to experience dipole-dipole repulsion with each other. The dipole-dipole form is:

$$\frac{u(r)}{k_B T} = a_2 \frac{1}{r^3} \tag{1}$$

where u is the potential, k_B is Boltzmann's constant, T is the thermal temperature, a_2 is the scaling constant, and r is the center to center distance of the particles. In our bi-disperse system, the average separation between small particles is $r_{ss} = 7.53\mu m$. Separation between large particles is $r_{ll} = 8.74\mu m$.

This system is often used to study interfacial colloids; Park et al. [1] published a study that precisely measures the form of the interparticle potential quantitatively using Monte Carlo methods and optical tweezers. We used particles from the same manufacturer (Invitrogen Corporation, Carlsbad, CA) as Park et al. and followed the same particle cleaning procedure. They report that for particles of size $D_P = 3.1\mu m$, the mean value of $\langle a_{2,P} \rangle = 5.1 \pm 2.4 \times 10^{-13} m^3$, where P subscripts indicate Park et al.'s values.

Within our bi-disperse system, the osmotic pressure is the same between large-large and small-small particles. Here the osmotic pressure is $-\frac{d^2u(r)}{dr^2}$. This allows us to write:

$$\frac{\langle a_{2,s}\rangle}{r_{ss}^5} = \frac{\langle a_{2,l}\rangle}{r_{ll}^5} = \frac{\langle a_{2,p}\rangle}{r_{pp}^5} \tag{2}$$

These equations are not linearly independent, so we extrapolate from our diameter-separation information ($[D_s, r_{ss}]$ and $[D_l, r_{ll}]$) to determine r_{pp} using D_P. We find $r_{pp} = 6.72\mu m$, $\langle a_{2,s}\rangle = 9.0 \times 10^{-13} m^3$, and $\langle a_{2,l}\rangle = 1.8 \times 10^{-12} m^3$.

For the main body of the text we use the average weighted by particle numbers of $\langle a_{2,s}\rangle$ and $\langle a_{2,l}\rangle$ for the entire suspension as $\langle a_2\rangle$. Forces are calculated as $F_{el.}(r) = -\frac{du}{dr} = \frac{3\langle a_2\rangle k_B T}{r^4}$.

6.4 Phenomenological Derivation

This section begins with the energy balance introduced in the main body (Eq. 1). In the first subsection we show how this equation is expanded to include the particulars of oscillatory shear. The second section lays out the details for quantifying bulk mechanical properties, such as yield.

6.4.1 Specifics of oscillatory shear

Briefly, as discussed in the main text, equation 1 quantifies energy accumulated in the system, TdS on the left hand side and the contributions from reversibly transferred and dissipated energy on the right hand side. Our experiments and simulations indicate that:

$$T\Delta S = F^* x/2 + f_d F x. \tag{3}$$

Here T is a fit constant that converts changes in entropy to changes in energy. S is the entropy of the entire system. F^* is a property of the material that quantifies how jammed the particles are via the total force experienced by a typical particle with its neighbors. It is calculated as: $F^* = \rho \int\int (-\frac{\partial u}{\partial r}) g(x,y) dxdy$, where ρ is the number density of particles, u is the inter-particle potential, and g(x,y) is the radial distribution function. Here f_d is the fraction of particles undergoing dissipative events detected via non-affine rearrangements. Non-affine events are detected via D^2_{min}. See Refs [2–4] for details on this calculation. Specifically, $f_d = N_d/N$, where N_d is the number of particles experiencing non-affine events and N is the number of total particles observed. The proscribed shear force and resultant displacement of the shearing surface are F and x respectively. We define the Δ operation as the difference between entropy at time t and the average entropy over an entire cycle of shear: $\Delta S = S(t) - \overline{S(t)}$.

We next summarize the specifics of our systems: most notably oscillatory shear and excess entropy. To apply equation 3 to the oscillatory shear cases considered in this paper, substitute in the time signals for shear surface displacement ($x(t) = x_0 sin(\omega t + \delta)$) and force ($F(t) = F_0 sin(\omega t)$) on the right-hand-side. On the left-hand-side, multiply by Nk_B/Nk_B:

$$Nk_B T\Delta(\frac{S}{Nk_B}) = \frac{F^* x_0}{2} sin(\omega t + \delta) + \frac{N_d}{N} F_0 sin(\omega t) x_0 sin(\omega t + \delta) \tag{4}$$

where ω is the frequency of the imposed force and δ is the resulting time lag between the imposed force and the resulting displacement. δ is an important physical parameter in rheology; it helps us to distinguish between solids, fluids, and everything in between. A fully elastic material has a $\delta = 0[rad]$; stress and strain are in phase as is seen from Hooke's law. A fully viscous material has a $\delta = \pi/2[rad]$; stress and strain are fully out of phase as is seen from Newton's law of viscosity[5].

In our experiments, changes in pressure are negligible. Therefore, changes in absolute entropy are approximately the same as those for excess entropy ($ds_2 \sim ds - ds_{I.G.} \sim ds_{total}$); the ideal gas entropy is not expected to change. Notice, entropy has changed to lower case 's' to represent quantities that are normalized by N and in units of k_B, which is convention. In simulations, entropy harmonics are directly calculated on $TS = E + PV$ because pressure, P, volume, V, and energy, E, are accessible[6–8]. Additionally, here we implement the product-to-sum trigonometric identity ($sin(u)sin(v) = (1/2)[cos(u-v) - cos(u+v)]$). Reorganizing gives:

$$\Delta s_2 = \frac{F^* x_0}{2Nk_B T} sin(\omega t + \delta) + \frac{N_d F_0 x_0}{2N^2 k_B T}\{cos(\delta) - cos(2\omega t + \delta)\}. \tag{5}$$

Equation 5 describes the evolution of a jammed system as it undergoes oscillatory shear and is fully non-dimensional. It is now apparent that the second term on the right-hand side (with N_d) has the second harmonic of the forcing frequency 2ω; this relation reproduces the frequency shift of the entropy signals in our simulations and experiments (main body Fig. 3a). The appearance of the second harmonic in the entropy signal captures well the transition to plasticity.

6.4.2 Connection to Rheology

We investigate the yield transition further by taking the ratio of the first and second harmonics within frequency domain of s_2, ($s_{2,h} \equiv \frac{FFT_{s_2}(2\omega)}{FFT_{s_2}(\omega)}$), which follows from equation 4 as:

$$s_{2,h}^2 = \frac{N_d}{N}\frac{F_0}{F^*}. \tag{6}$$

Equation 6 is visualized in figure 4a of the main text. This scaling is quadratic because N_d and F_0 scale linearly with each other (Fig. 3). The square of $s_{2,h}$ in equation 6, is included so that linear relationships are retained throughout.

From here we revisit an idea posited by Falk and Langer (Ref.[9]): relaxation events are due to a local buildups of elastic energy that suddenly release (i.e. $G'' \propto N_d G'$). Recently quantified for above yield cases in Ref.[3] and here expanded to below yield, $G'' = \frac{2a^2}{\pi A} N_d G'$, where a is the first peak distance of g(r) and A is the area of observation. Substituting this equation into equation 6 for N_d gives:

$$\frac{G''}{G'} = \frac{2Na^2}{\pi A}\frac{F^*}{F_0}s_{2,h}^2 = \frac{2\phi}{\pi^2}\frac{F^*}{F_0}s_{2,h}^2 \tag{7}$$

which allows us to relate the bulk material response directly to measurable microstructural properties without the use of fitting parameters. Equation 7 is visualized in Fig. 4b&c. ϕ quantifies particle density as $\phi = \pi N a^2/A$, which implicitly takes a as an effective particle diameter. This relation reveals that the yielding transition of jammed materials is specified by four dimensionless groups based on imposed force, particle density, a memory based dimensionless entropy, and the bulk response.

References

1. Park, B. J., Vermant, J. & Furst, E. M. Heterogeneity of the electrostatic repulsion between colloids at the oil–water interface. *Soft Matter* **6,** 5327–5333 (21 2010).
2. Keim, N. C. & Arratia, P. E. Yielding and microstructure in a 2D jammed material under shear deformation. *Soft Matter* **9,** 6222–6225 (27 2013).
3. Keim, N. C. & Arratia, P. E. Mechanical and Microscopic Properties of the Reversible Plastic Regime in a 2D Jammed Material. *Phys. Rev. Lett.* **112,** 028302 (2 Jan. 2014).
4. Keim, N. C. & Arratia, P. E. Role of disorder in finite-amplitude shear of a 2D jammed material. *Soft Matter* **11,** 1539–1546 (8 2015).
5. Larson, R. *The structure and rheology of complex fluids* (Oxford University Press, 2010).
6. Ono, I. K. *et al.* Effective Temperatures of a Driven System Near Jamming. *Phys. Rev. Lett.* **89,** 095703 (9 Aug. 2002).
7. Sciortino, F., Kob, W. & Tartaglia, P. Inherent Structure Entropy of Supercooled Liquids. *Phys. Rev. Lett.* **83,** 3214–3217 (16 Oct. 1999).
8. Bonnecaze, R. T., Khabaz, F., Mohan, L. & Cloitre, M. Excess entropy scaling for soft particle glasses. *J. Rheol.* **64,** 423–431 (2020).
9. Falk, M. L. & Langer, J. S. Dynamics of viscoplastic deformation in amorphous solids. *Phys. Rev. E* **57,** 7192–7205 (6 June 1998).